THE JOURNAL OF BIOLOGICAL CHEMISTRY
Vol. 275, No. 21, Issue of May 26, pp. 16174–16182, 2000

Printed in U.S.A.

Substrate Recognition by the Lyn Protein-tyrosine Kinase

NMR STRUCTURE OF THE IMMUNORECEPTOR TYROSINE-BASED ACTIVATION MOTIF SIGNALING REGION OF THE B CELL ANTIGEN RECEPTOR*

Received for publication, November 10, 1999, and in revised form, February 15, 2000
Published, JBC Papers in Press, March 20, 2000, DOI 10.1074/jbc.M909044199

Beverly S. Gaul, Marietta L. Harrison, Robert L. Geahlen, Robert A. Burton, and Carol Beth Post‡

From the Department of Medicinal Chemistry and Molecular Pharmacology, Purdue University, West Lafayette, Indiana 47907-1333

The immunoreceptor tyrosine-based activation motif (ITAM) plays a central role in transmembrane signal transduction in hematopoietic cells by mediating responses leading to proliferation and differentiation. An initial signaling event following activation of the B cell antigen receptor is phosphorylation of the CD79a (Ig-α) ITAM by Lyn, a Src family protein-tyrosine kinase. To elucidate the structural basis for recognition between the ITAM substrate and activated Lyn kinase, the structure of an ITAM-derived peptide bound to Lyn was determined using exchange-transferred nuclear Overhauser NMR spectroscopy. The bound substrate structure has an irregular helix-like character. Docking based on the NMR data into the active site of the closely related Lck kinase strongly favors ITAM binding in an orientation similar to binding of cyclic AMP-dependent protein kinase rather than that of insulin receptor tyrosine kinase. The model of the complex provides a rationale for conserved ITAM residues, substrate specificity, and suggests that substrate binds only the active conformation of the Src family tyrosine kinase, unlike the ATP cofactor, which can bind the inactive form.

The immunoreceptor tyrosine-based activation motif (ITAM)[1] plays a central role in transmembrane signal transduction in hematopoietic cells. Since the recognition of this motif (1), it has been identified in the cytoplasmic domains of numerous antigen and Fc receptors, as well as certain viral proteins (2, 3). Although the ITAM occurs on many receptors, and in multiple copies in some instances, the transduced signals mediated by different ITAM regions can lead to distinct pathways. Only 6 residues of the approximately 26-residue-long sequence ((D/E)X_7(D/E)X_2YX_2(L/I)X_7YX_2(L/I)) are conserved across receptors, suggesting that the functional specificity of different ITAMs may be determined by the 20 nonconserved residues (2). Neither the basis for the evolutionary pressure to conserve these 6 residues nor the structural determinants for specificity of ITAM are completely understood.

We report here the first structure determination of an ITAM region bound as a substrate to a Src family tyrosine kinase. Lyn (4, 5), one of nine members of the Src family, associates with the B cell antigen receptor following activation by antigen binding (6, 7). In an initial event of B cell signaling, Lyn preferentially phosphorylates the first tyrosine of the CD79a ITAM (8–10). Asymmetrical phosphorylation of the two tyrosines of the ITAM has also been demonstrated for phosphorylation by Fyn, another Src family kinase (11), and for *in vivo* phosphorylation (12). After phosphorylation, the ITAM becomes a membrane docking site for the SH2 domains of the Syk protein-tyrosine kinase to further signaling in the B cell (10, 13, 14). Src family tyrosine kinases are targets for drug discovery in allergic diseases, autoimmunity, transplantation rejection, and cancer (15, 16). As no structure of a bound substrate has been previously determined, and few natural substrates are defined for these kinases, the structure of ITP reported here is potentially a useful template in drug design efforts.

The complex between the Lyn tyrosine kinase and a 12-residue peptide derived from the ITAM region of CD79a, acet-D^{178}ENLYEGLNLDD-NH_2, was examined using exchange-transferred nuclear Overhauser effect spectroscopy (et-NOESY). The resulting NMR structure of the ITAM substrate was docked onto the crystallographic structure of an activated Src family kinase (17) for the purpose of gaining insight into ITAM specificity determinants and Src kinase function in signaling. The results suggest that ITAM substrate binds in a cleft between the two lobes of the kinase domain similar to the binding of cyclic AMP-dependent protein kinase peptide inhibitors (18). This mode of binding differs from that of a peptide substrate bound to the insulin receptor kinase (19). The complex model of ITAM-Lck provides a rationale for conservation of some of the conserved residues of the ITAM, the substrate specificity of Lyn, and suggests a possible role of substrate binding to activated Src in stabilization of the activated conformation.

EXPERIMENTAL PROCEDURES

GST-kLyn Expression—A cDNA coding for the catalytic domain of Lyn, kLyn, beginning at the codon for Arg^{221} and extending through the polyadenylation site, was isolated from a B cell λ-zap cDNA expression library by screening with anti-phosphotyrosine antibodies. The Lyn cDNA was subcloned into the *Xba*I-*Xho*I site of the pGEX-KG vector (20) to allow expression of the kinase in *Escherichia coli* as a glutathione *S*-transferase (GST) fusion protein. The kLyn fusion protein was isolated from lysates of isopropyl-1-thio-β-D-galactopyranoside-induced cells by chromatography on glutathione-agarose (Sigma). The GST-kLyn fusion product was eluted with two applications of 10 mM gluta-

* The work was supported by National Institutes of Health Grants K04GM00661 and R01GM39478 (to C. B. P.), R01CA37372 (to R. L. G.), and R01GM48099 (to M. L. H.). The costs of publication of this article were defrayed in part by the payment of page charges. This article must therefore be hereby marked "*advertisement*" in accordance with 18 U.S.C. Section 1734 solely to indicate this fact.

‡ To whom correspondence should be addressed: Dept. of Medicinal Chemistry, Purdue University, West Lafayette, IN 47906-1333. Tel.: 765-494-5980; Fax: 765-496-1189; E-mail: cbp@cc.purdue.edu.

[1] The abbreviations used are: ITAM, immunoreceptor tyrosine-based activation motif; ITP, ITAM peptide substrate, residues 178–189; kLyn, catalytic domain of Lyn tyrosine kinase, residues 221–491; NOE, nuclear Overhauser effect; et-NOESY, exchange-transferred nuclear Overhauser effect spectroscopy; ROESY, rotating frame nuclear Overhauser enhancement spectroscopy; TOCSY, total correlation spectroscopy; SH, Src homology; GST, glutathione *S*-transferase; cAPK, cyclic AMP-dependent protein kinase; IRK, insulin receptor tyrosine kinase.

ITAM	**D**XX**Y**XX**L**XXXXXXX**Y**XX**L** **E** **I**
ITP	D**E**N**LYEGL**NLDD
CD79a	D**E**N**LYEGL**NLDDCSM**Y**ED**I**
CD79b	E**D**H**LYEGL**DIDQ
Peptide library	DEEIYEELX
Phage display	DXIYEXLP E L D

SCHEME 1. **ITAM consensus sequence and related sequences.** The conserved residues from the ITAM region of CD79a (Ig-α) and CD79b (Ig-β) in the B cell antigen receptor are in *bold type*. Consensus substrate sequences recognized by Lyn determined either from a combinatorial peptide library or by phage display are also shown.

thione in phosphate-buffered saline, dialyzed against phosphate-buffered saline, and concentrated. Protein concentration was estimated from the 280-nm UV absorbance using an extinction coefficient value of 55.3×10^3 liters cm^{-1} mol^{-1}.

Peptide Phosphorylation—The peptides were synthesized by the Purdue University Peptide Synthesis Laboratory with solid phase synthesis, and purified by fast protein liquid chromatography using a Pharmacia C_2-C_{18} column and a solvent system of 0.1% trifluoroacetic acid in H_2O (solution A) and 0.1% trifluoroacetic acid in 95% HPLC-grade acetonitrile, 5% H_2O (solution B). For analysis of the *in vitro* peptide phosphorylation, the peptides acet-DENLYEGLNLDD-NH_2 and acet-ENLYEGLNLDDCSMYEDI-NH_2 (160 μM) were incubated with expressed kLyn-GST fusion protein in reactions containing 5 mM HEPES, pH 8.4, 10 mM $MnCl_2$ 5 mM *p*-nitrophenylphosphate, 50 μM [γ-^{32}P]ATP, and 1 mM 2-mercaptoethanol for the times indicated. Reaction components were separated by electrophoresis on an 40% alkaline-polyacrylamide gel as described (21). Phosphopeptides were recovered from the gel and incubated for 2 h with 10 μg of *Staphylococcus aureus* V8 protease in 50 mM NH_4CO_3, pH 7.8, at 37 °C, followed by an additional 2-h incubation with a freshly added 10 μg of protease. The resulting samples were again separated by 40% alkaline-PAGE. Phosphopeptides were visualized by autoradiography.

Enzyme Assay for Peptide Phosphorylation—Phosphorylation of peptides by kLyn-GST fusion protein and the accompanying production of ADP were monitored by enzymatic coupling to the oxidation of NADH using phosphoenolpyruvate, pyruvate kinase, and lactate dehydrogenase (Sigma) (22). The disappearance of NADH was monitored at 340 nm at room temperature for 10 min. The K_m values were calculated from rates estimated from the linear time-dependent change in absorbance. Each reaction contained 100 mM HEPES, pH 7.5, 20 mM $MgCl_2$, 1 mM ATP, 4 mM phosphoenolpyruvate, 150 μM NADH, 70 nM Lyn kinase, 14 units of pyruvate kinase, and 20 units of lactate dehydrogenase in a final volume of 1 ml. The peptide concentration was varied from 1 to 100 μM. Lyn was activated by preincubation with 20 mM $MgCl_2$ and 1 mM ATP for 30 min at 4 °C.

NMR Spectroscopy—TOCSY (23), ROESY (24), and et-NOESY using WATERGATE solvent suppression (25) were run at 5 °C in a Shigemi™ tube with a Varian VXR 500 or a Varian Unity Plus 600 spectrometer equipped with a pulsed *z*-field gradient unit. The mixing time for TOCSY was 70 ms and for ROESY was 300 ms.

Peptide samples were prepared in 90% H_2O, 10% D_2O, 0.13 M sodium phosphate, 0.14 NaCl, pH 7.2. The ITP peptide ^{1}H resonances were assigned from the TOCSY and ROESY data using sequential methods, and the assignments have been deposited with the BioMagRes data base. The amide and α resonances of Asp^{11} and Asp^{12} were degenerate and not assigned sequentially.

Peptide/enzyme complex samples, 1 mM peptide and 0.2 mM GST-Lyn, were prepared in 90% H_2O, 10% D_2O, 0.13 M sodium phosphate, 0.14 NaCl, pH 7.2. WATERGATE-et-NOESY experiments were conducted with a mixing time of 300 ms, a recycle time of 1.5 s, and signal averaging of 32 transients collected for 512 t1 increments. Control samples of glutathione *S*-transferase protein in the presence of ITP (1:5 ratio) and ITP alone were run under the same conditions. The spectra were processed using nmrPipe (26).

NMR Structure Determination—Cross-peak intensities in the et-NOESY spectrum were quantified (27), and then classified as strong (1.8–2.7 Å), medium (1.8–3.3 Å), or weak (1.8–5.0 Å) distance restraints. The reference cross-peak intensity was from two fixed-distance

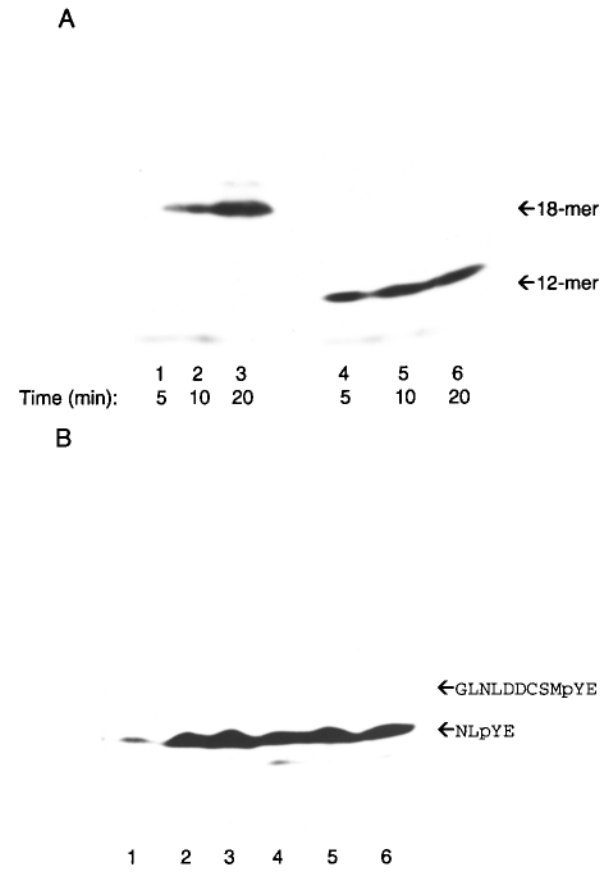

FIG. 1. **Phosphorylation of CD79a ITAM peptides by kLyn.** *A*, phosphorylation of ENLYEGLNLDDCSMYEDI (18-mer) and DENLYEGLNLDD (12-mer). Peptides were phosphorylated *in vitro* with kLyn for the indicated times and then separated by 40% alkaline-PAGE. The migration positions of the corresponding peptides are indicated. *B*, location of phosphorylation sites on the ITAM 18-mer. Phosphopeptides isolated from the gel illustrated in *panel A* were digested with *S. aureus* V8 protease and the reaction products separated by 40% alkaline-PAGE. The migration of the two cleavage products are indicated.

proton pairs: the H_δ-H_ϵ cross-peaks from Tyr^5 and the H_γ-H_γ cross-peak from Asn^3. Restrained energy minimization and molecular dynamics calculations from X-PLOR 3.1 (28) started from initial coordinates corresponding to either an ideal α-helix or an extended chain. Assignment of different initial velocities generated 200 structures. The electrostatic energy terms were excluded from the X-PLOR force field (topallhdg.pro and parallhdg.pro files), and the NOE distances were restrained to a soft-square-well potential function using a force constant of 50 kcal mol^{-1}Å^{-2}. High temperature dynamics with a l-fs time step and coupling to 1000 K for 30 ps was followed by cooling at a linear rate to 100 K over a period of 15 ps, and 1200 steps of Powell energy minimization. Each structure was then optimized by 2000 steps of Powell energy minimization against a more physically accurate force field, the CHARMM22 force field (topallh22x.pro and parallh22x.pro files) (29), including a coulombic electrostatic potential term with a distant-dependent dielectric constant. The 20 best structures out of 200 were selected based on low NOE energy, few NOE violations, and good ϕ,ψ geometry defined using PROCHECK (30). No distinction was found for the two initial conformations in terms of total energy, NOE restraint energy, or final conformation.

Docking of ITP—ITP was manually docked onto the known structure of activated Lck tyrosine kinase (Protein Data Bank code 3lck) (17) using the graphics program QUANTA, followed by distance-restrained molecular dynamics and energy minimization with CHARMM (31). The manual docking of ITP onto kLck was guided by known structures of the complex of cyclic AMP-dependent protein kinase (cAPK) with a peptide inhibitor and ATP (Protein Data Bank code 1atp) (18), and the insulin receptor tyrosine kinase (IRK) complex with a peptide substrate and AMP-PNP (Protein Data Bank code 1ir3) (19). The three kinase structures were superpositioned by a least-squares fit of the main chain atoms in the catalytic segment and in the core secondary structure of

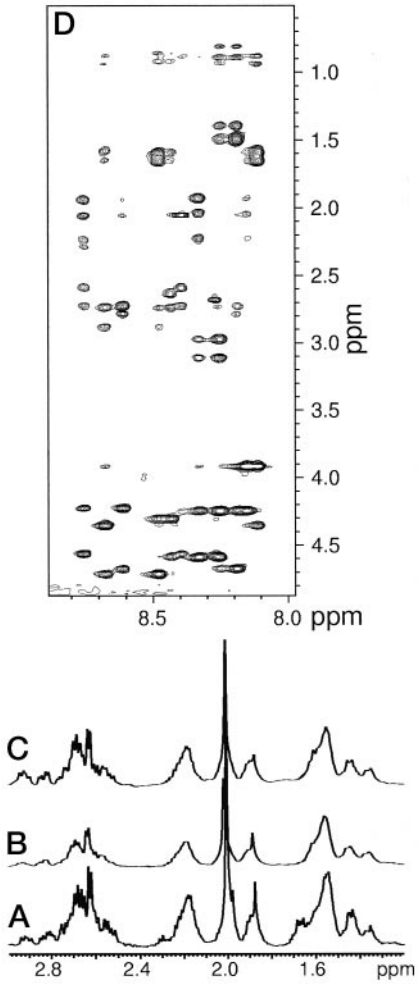

FIG. 2. *A–C*, aliphatic region of the one-dimensional ^{1}H NMR spectrum of ITP. *A*, 0.5 mM ITP in the absence of kLyn. *B*, broadened resonances of 0.5 mM ITP in the presence of 0.15 mM kLyn. *C*, addition of lavendustin, dissolved in D-acetic acid to give 0.15 mM, to sample shown in *B* reverses the broadening of ITP resonances. The data were multiplied by an exponential function with a line broadening factor of 2. *D*, amide region of the et-NOESY spectrum of 1 mM ITP in the presence of 0.2 mM kLyn. The spectrum was measured in 90% H_2O, 10% D_2O using a WATERGATE sequence, 0.13 M sodium phosphate, 0.14 NaCl, pH 7.2. The spectrum was collected for 300 ms of mixing time, with 32 transients, 2000 × 512 data points, and processed using Gaussian apodization in both dimensions.

the C-lobe subdomain. An NMR ITP structure was then aligned with either the cAPK or IRK peptide by superposition of the main chain atoms of the acceptor residues. These two template structures gave distinct initial positions for ITP on the kLck surface. The superposition was followed by manual, graphical manipulation of ITP to remove obvious steric conflicts.

Each of the 20 best ITP NMR structures were aligned with the coordinates for both of the two manually docked models by superposition of the ITP main chain atoms of residues 1–7. Each model was subjected to 450 steps of restrained energy minimization, followed by 5-ps molecular dynamics at an initial temperature of 500 K and cooled to 300 K over a 5-ps period, and then optimized by 150 steps of Powell energy minimization. NMR distance restraints were applied in all molecular mechanics and dynamics with a force constant of 100 kcal/mol/Å and a soft-square-well potential. The backbone atoms of kLck were harmonically constrained to their crystallographic coordinates with a force constant of 100 kcal/mol/Å^2, while residues with no atoms in a 10-Å radius of any ITP atom were fixed in space.

RESULTS AND DISCUSSION

ITAM Phosphorylation by Lyn in Vitro—To explore the substrate specificity of Lyn for the phosphorylation of the two ITAM tyrosine residues of CD79a, we prepared peptides of

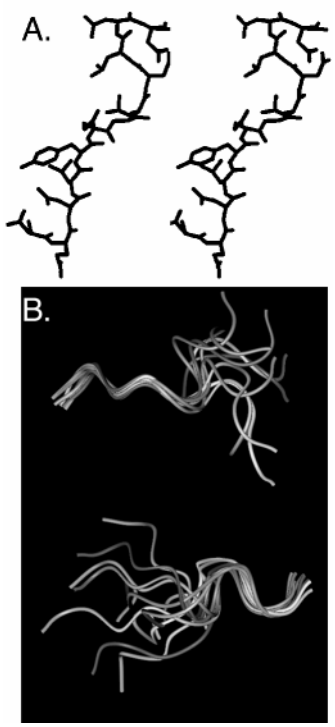

FIG. 3. *A*, stereoview of a representative structure of bound ITP. *B*, 10 of the 20 selected NMR structures of bound ITP. The main chain atoms of either residues 1–7 (*top*) or residues 8–12 (*bottom*) are superpositioned. These figures and other ribbon or vector drawings were generated using the QUANTA program.

sequence acet-D^{178}ENLYEGLNLDD-NH_2 (ITP) and acet-E^{179}NLYEGLNLDDCSMYEDI-NH_2 to use as substrates for *in vitro* phosphotransferase assays. These peptides correspond in sequence to the CD79a ITAM (Scheme 1) and contain either one or both of the conserved ITAM tyrosines. Peptides were incubated in the presence of [γ-^{32}P]ATP with the catalytic domain of Lyn (kLyn), and the phosphopeptides separated from the reaction components by electrophoresis. kLyn was capable of catalyzing the phosphorylation of both peptides (Fig. 1). Each phosphopeptide was then recovered from the gel and digested with *S. aureus* V8 protease under conditions in which proteolysis is restricted to the COOH termini of glutamate residues. This separates the 18-residue peptide into two distinct fragments, each of which contains one of the ITAM tyrosines (Fig. 1). Only a single phosphopeptide was generated from the 18-residue peptide, indicating that only a single tyrosine had been phosphorylated to a detectable extent. The migration of this phosphopeptide on the alkaline gel was identical to that of the phosphopeptide generated from the 12-residue peptide, which contains only the amino-terminal ITAM tyrosine. This result confirms previous results indicating that Src family kinases exhibit a strong preference for phosphorylation of the first of the two ITAM tyrosines.

ITP Structure Determination—The structure was determined of ITP bound in the active site of Lyn. ITP contains the amino-terminal ITAM tyrosine of CD79a (Scheme 1). The form of Lyn was a GST fusion protein containing the Lyn catalytic domain, kLyn. kLyn is expressed in its activated, phosphorylated form as determined by Western blotting with anti-phosphotyrosine antibodies. ITP is phosphorylated by kLyn, with K_m equal to 13 μM as measured by a coupled enzymatic assay for phosphorylation (data not shown).

NMR spectra of free ITP and ITP in the presence of kLyn are shown in Fig. 2 (*A* and *B*, respectively). The broadening of the ^{1}H resonances from ITP upon titration with kLyn is due to the

TABLE I
Average pairwise root mean square difference of main chain atoms N, Cα, and C for the 20 best ITP structures

Residues	Main chain	Heavy atom
1–12	1.95	2.60
1–7	0.69	0.80
8–12	0.71	1.76

averaging of the linewidths from the bound and free states of ITP when exchange is fast with respect to chemical shift differences. Moreover, assuming diffusion-limited binding, the dissociation rate is estimated to be 10^3 s^{-1}. This rate is significantly faster than cross-relaxation in the complex, so that exchange-transferred NOE interactions are observed and distances may be readily estimated from et-NOE intensities (32).

That ITP binds specifically to kLyn was tested by competition with lavendustin, a high affinity, active site inhibitor of Src family tyrosine kinases (33, 34). Addition of lavendustin to a sample containing ITP and kLyn (Fig. 2*C*) results in reversal of the broadened ITP resonances to the narrower linewidths characteristic of the free state of ITP. This reversal by competition with lavendustin indicates that ITP binds specifically to kLyn at the high concentrations required for the NMR experiment.

Examination of the amide region of the et-NOESY spectrum shown in Fig. 2*D* finds a significant number of well resolved cross-peaks resulting from intramolecular NOE interactions of ITP bound to kLyn. A NOESY spectrum of ITP measured with identical parameters either in the absence of protein, or in the presence of glutathione *S*-transferase, showed only a small number of intraresidue NOEs between protons separated by a single dihedral angle. These control experiments confirm that the NOE interactions measured in the presence of kLyn reflect the structure of ITP bound to kLyn.

Exchange-transferred NOESY cross-peaks, categorized as strong, medium, or weak intensities, provided 107 structurally useful distance restraints for ITP, with 53 of the distance restraints derived from NOE interactions involving amide protons. Many of the NOE interactions involving Asp^{11} and Asp^{12} could not be assigned unambiguously, and therefore were not interpreted for distance restraints in the structure determination. ITAM residues 1 and 3–10 have one to five midrange NOE interactions to a non-neighboring residue. The occurrence of midrange NOE interactions over most of the peptide indicates that a reliable model of the bound structure may be obtained using the et-NOESY method of structure determination (35). The energy averaged over the 20 best *in vacuo* ITP structures generated by simulated annealing and restrained molecular dynamics was -131.0 ± 12 kcal/mol, and the average NOE energy was 1.4 ± 0.24 kcal/mol. Interproton distances in the 20 best structures did not violate the NOE restraint distances by more than 0.2 Å, and the average number per structure of NOE violations greater than 0.1 Å was 0.6.

NMR Structure of Bound ITP—A representative structure of bound ITP is shown in Fig. 3*A*. The kinase substrate peptide binds in an irregular helix-like conformation with most of the side chains oriented in one direction. The polypeptide backbone in this enzyme-substrate complex is not extended, unlike the peptide structure of phosphotyrosine-containing peptides recognized by SH2 and phosphotyrosine binding domains.

The structure of ITP bound to kLyn for residues 1–7 and 8–12 is well determined by the NMR data, but the main chain conformation varies across Gly^7 despite an NOE distance restraint between Gly^7 and Asn^9. Ten models from the set of 20 best *in vacuo* NMR structures are superpositioned in Fig. 3*B*. The precision of the NMR structures is high when the main chain atoms of either residues 1–7 or residues 8–12 are superpositioned, while the precision is lower when full-length ITP is superpositioned (Table I). The average root mean square difference from the average structure when residues 1–7 are superpositioned was 0.80 and 0.69 Å for all non-hydrogen atoms and main chain atoms, respectively, and for residues 8–12 was 1.76 and 0.71 Å, respectively. When full-length ITP is compared, the values were 2.60 and 1.95 Å, respectively. All structural models satisfy the Gly^7-Asn^9 NOE restraint. As such, the single midrange restraint on Gly^7 is not sufficient for defining the backbone conformation of this residue with high precision. Since we find no experimental evidence, such as differential linewidths (36), to support actual conformational disorder in the complex, the heterogeneity in the NMR models likely reflects a limitation of the NMR data to define the bound state structure, rather than a property of that binding.

FIG. 4. **Ribbon drawing of the kinase domains of down-regulated Hck (*green*) and activated Lck (*blue*).** The two structures are overlaid by a least-squares superposition of main chain atoms in the C-lobe corresponding to residues 425–515 in Src, seen on *bottom* in this view. This superposition emphasizes the difference in the relative orientation of the N-lobe (*top*) and the activation segment (*yellow* in Hck and *gray* in Lck) between the down-regulated and active forms of the Src family kinases.

Model for the ITAM Substrate-Kinase Complex—Structural information on kLyn is not obtained by the et-NOE method because the linewidths of the 56-kDa kLyn-GST protein are too broad to measure accurately. To gain insight into the mechanism of recognition and enzymatic activation of Src family tyrosine kinases, the ITAM substrate-kinase complex was modeled using a known structure of a phosphorylated Src family tyrosine kinase domain, that of Lck (17). This kinase domain of Lck (kLck) is ideal for modeling the kLyn-ITP complex since Lyn and Lck have a 75% sequence identity in the catalytic domain (4), and comparative modeling methods have been shown to be reliable with this high sequence identity (37–40). Moreover, the crystallographic structure of Lck is the activated

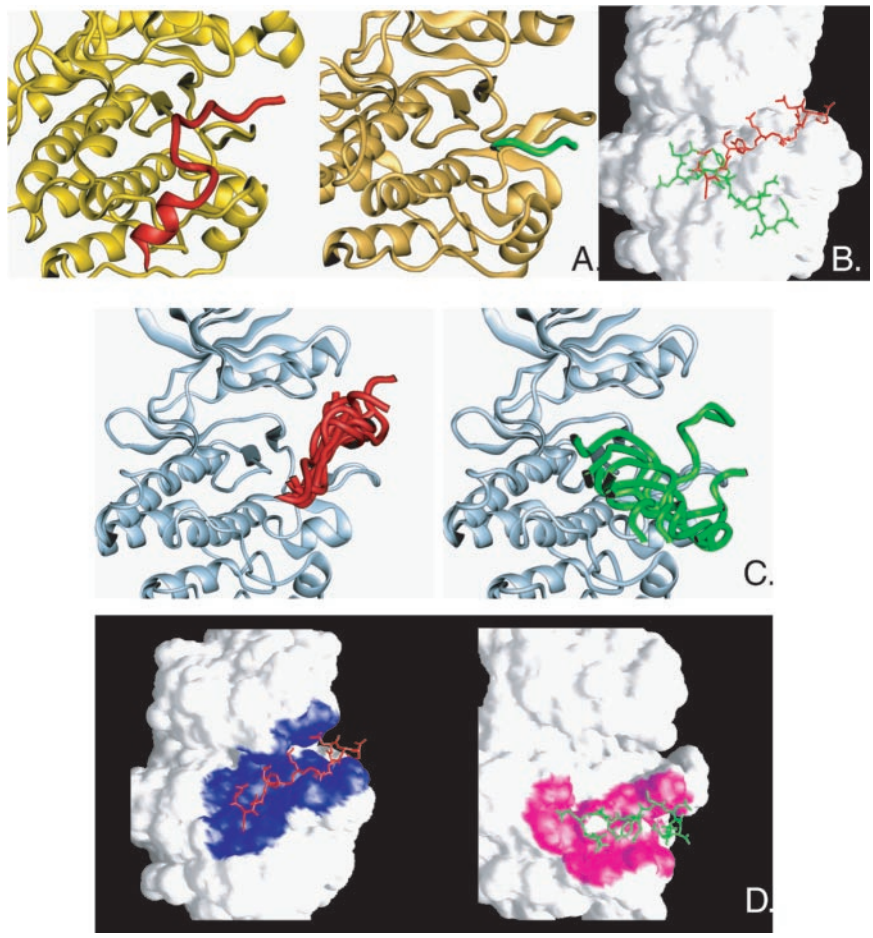

FIG. 5. **Modeling of ITP binding to kLck based on template structures of cAPK (*left column*) or IRK (*right column*).** *A*, ribbon drawings of the complex between cAPK and a peptide inhibitor (*red*, *left*), and between IRK and a peptide substrate analogue (*green*, *right*). *B*, molecular surface drawing from GRASP of kLck with an NMR structure of ITP docked based on the cAPK peptide template (*red*) or the IRK peptide template (*green*). *C*, docked ITP structures after conformational relaxation by distance-restrained molecular dynamics starting from the cAPK template (*red*, *left*) or IRK template (*green*, *right*). *D*, molecular surface colored according to close contact between ITP and kLck for the cAPK template (*blue surface*, *left*) or IRK template (*magenta surface*, *right*). A *white surface* appears when no ITP atom is within 5 Å of any kLck atom. These molecular surfaces and others were generated using GRASP.

form of the kinase domain in which Tyr^{394} (Tyr^{416} in Src numbering),[2] is phosphorylated, analogous to the form of kLyn used in this NMR study.

All protein kinases have common structural features despite low sequence similarity (41). The kinase domain comprises two subdomains: a smaller amino-terminal lobe (*top* in Fig. 4), and a larger, COOH-terminal lobe (*bottom* in Fig. 4). The activation segment lies at the interface of these subdomains, and is differentially color-coded in Fig. 4. In the structure of kLck (*blue*), $Tyr^{394(416)}$ is phosphorylated, and the activation segment (*gray*) was well ordered in the initial crystallographic determinations. By contrast, in the earlier crystallographic structures of Hck or Src kinase (42–44) in the down-regulated form, where Tyr^{416} is not phosphorylated, the activation segment is disordered, although recent results (45, 46) define the conformation for this segment shown in Fig. 4 (*yellow* activation segment and *green* kinase protein).

Structures are known for three kinases with a bound peptide ligand. The initial positioning of ITP was guided by two of these two kinase-peptide complexes and the shape of the kinase surface visualized with the program GRASP (47). In the complex of cAPK, the peptide inhibitor binds partially in the cleft between the N- and C-lobes of this Ser/Thr kinase (18, 48) (Fig. 5*A*, *left*), similar to peptide binding of phosphorylase kinase (49). The peptide substrate in the tris-phosphorylated IRK complex binds in a different orientation (Fig. 5*A*, *right*), and contacts the C-lobe adjacent to the cleft with the acceptor tyrosine hydrogen-bonded to active site residues (19). Electron density is observed for only 6 of the 18 residues of the IRK peptide substrate. Thus, ITP was modeled in two orientations on the surface of kLck, one in the interlobe cleft based on the position of the cAPK peptide inhibitor (Fig. 5*B*, *red*), and a second one oriented mostly contacting the C-lobe in a fashion analogous to the IRK peptide substrate (Fig. 5*B*, *green*) (see "Experimental Procedures"). For the cleft model, ITP lies on the opposite side of the activation segment compared with the C-lobe model. Each of the 20 et-NOE structures defined in the absence of the protein was positioned in either orientation, and subjected to distance-restrained molecular dynamics and energy minimization to give 20 conformationally relaxed structures in each orientation.

The results from modeling ITP in the two orientations differed significantly. The 20 structures of ITP docked in the interlobe cleft are in good agreement with the NMR data, and the complexes have good structural properties (Table II). These cleft models satisfy the NMR restraints better than the isolated ITP structures before docking; the average E_{NOE} for the 20 docked ITP structures is 0.7 ± 0.2 kcal/mol, compared with 1.4 ± 0.2 kcal/mol, respectively. In contrast, docking of ITP to the C-lobe resulted in an average E_{NOE} of 4.1 ± 3.3 kcal/mol, in poorer agreement with the NMR data. The influence on the NOE energy for the complex is the result of the intermolecular energy of interaction. There are no added restraint energies for docking. During refinement by restrained molecular dynamics, the cleft-bound models converge to similar conformations (Fig. 5*C*, *red*) and have several common intermolecular interactions, while the C-lobe models are substantially less precise (Fig. 5*C*, *green*). ITP modeled in the cleft has good chemical and structural complementarity with the kinase; the average number of intermolecular hydrogen bonds is 10 ± 3, in contrast to 7 ± 2 for the C-lobe docked models. Steric complementarity is illustrated in Fig. 5*D* by color coding the surface for regions of close

[2] Amino acid numbers shown in parentheses are c-Src numbering.

TABLE II
Results of the docking of ITP to kLck with initial positions either in the interlobe cleft of kLck, based on cAPK binding, or on the C-lobe based on IRK binding

Initial docking was followed by distance-restrained molecular dynamics and energy minimization to conformationally relax the complex. Values are averaged over the 20 selected structures.

Structure	$\langle E_{NOE} \rangle^a$	⟨Violations > 0.1⟩	⟨Intermolecular H bonds⟩	⟨Contact SA⟩[b]
	kcal/mol	*Å*		*Å²*
ITP alone	1.4 ± 0.2	0.6	NA[c]	NA
Cleft ITP · kLck[a]	0.7 ± 0.2	0	10 ± 3	1455 ± 180
C-lobe ITP · kLck[b]	4.1 ± 3.3	0.6	7 ± 2	1000 ± 230

[a] Quadratic well potential function, 50 kcal/mol/Å force constant.
[b] Surface area (SA) buried upon forming the ITP complex.
[c] NA, not available.

intermolecular contact. For ITP binding in the cleft, the *blue* contact surface (Fig. 5*D*, *left*) is continuous around the peptide, while the *magenta* surface in the case of ITP binding on the C-lobe (Fig. 5*D*, *right*) is interrupted by patches of uncolored area where the ITP and kinase residues are not in close contact. The average accessible surface area (1.4-Å probe radius) of kLck contacted by ITP is 1455 ± 180 Å^2 for the cleft model, and 1000 ± 230 Å^2 for the C-lobe model. Importantly, after refinement with ITP docked in the cleft, the acceptor tyrosine, Tyr^5, remains in the active site, while refinement of complexes with ITP oriented on the C-lobe results in Tyr^5 moving away from the active site and having little intermolecular contact.

Taken together, the results summarized in Table II and Fig. 5 strongly favor the cleft model for binding of ITP. The good agreement with the NMR data and the soundness of the structural features suggest that Src family kinases bind the ITAM substrate in the cleft region between the N- and C-lobes, similar to peptide binding in cAPK and unlike that in IRK, despite the closer protein structural similarity between IRK and Lck. The reason for the different orientations in substrate binding observed in the crystallographic structures for cAPK and IRK is not clear. It is of interest to note in this regard that, in the IRK complex, the peptide substrate occupies the site where the unphosphorylated activation segment is located in the down-regulated form of IRK. That is, the IRK peptide residues Asp^9 (the P−1 position) and Tyr^{10} (the P site) closely mimic the IRK residues Asp^{1161} and Tyr^{1162} in the activation segment of the unphosphorylated kinase. It is also the case for the tris-phosphorylated IRK complex that cleft residues of IRK at the end of helix C (1038, 1039, and 1042) and on the activation segment (1166, 1167, and 1168) are in close contact with neighboring molecules in the crystal, which could interfere with cleft binding by a ligand by blocking access to this site. Although the different orientations of substrate binding have been considered to distinguish Ser/Thr kinases from Tyr kinases (50), the cleft model proposed here would support a general substrate binding mode that is conserved among protein kinases.

Hereafter, we consider only the cleft model of ITP bound to kLck, given the results summarized in Table II. We describe in the remainder of this section the intermolecular interactions (Table III), which occurred with high frequency in the 20 docked and conformationally relaxed structures, and illustrate these interactions using one of the models (Fig. 6).

Catalytic Interactions—Residues of ITP are well positioned for catalysis in the model of ITP-kLck. Fig. 6*B* illustrates some of the hydrogen bond interactions between ITP and the kinase active site residues. The acceptor tyrosine, Tyr^5, interacts with Asp$^{364(386)}$ and Arg$^{366(388)}$, while Asp^1 interacts with Arg$^{366(388)}$. Asp^{364}, conserved among all known protein kinases, is thought to play the role of catalytic base during phosphoryl transfer (10). An analogous interaction was observed in the IRK kinase-peptide complex between Asp^{1132} and the acceptor tyrosine of that peptide (19). Further, in the model of the ITP-kLck complex, Tyr^5 is well oriented with the respect to what is known about binding the ATP cofactor. The docking and molecular dynamics refinement of ITP were done in the absence of ATP. When ATP from the cAPK structure (48) was positioned in the active site of the ITP-kLck model structure according to a least-squares superposition of the C-lobe of the kinase domain, Tyr^5 hydroxyl was found (Fig. 6*C*) to be oriented in a near-optimal position for nucleophilic attack of the nucleotide γ-phosphate group. Thus, the docking of ITP to kLck resulted in an excellent model for the catalytically active complex.

TABLE III
Intermolecular interactions of the ITAM region of CD79a from the cleft model of ITP and kLck

Amino acid numbers for the kinase interactions refer to kLck numbering, and those shown in parentheses are cSrc numbering.

ITP	Kinase interaction
Asp^1	Arg$^{366(388)}$
Glu^2	Lys$^{405(427)}$, Asn$^{446(468)}$
Asn^3	Arg$^{366(388)}$
Leu^4	Phe$^{256(278)}$
Tyr^5	Asp$^{364(386)}$, Arg$^{366(388)}$
Glu^6	Gln^{255} (Cys^{277})
Leu^8	Leu$^{385(407)}$, Gly$^{399(421)}$, Ala$^{400(422)}$, Phe$^{402(424)}$
Asn^9	Lys$^{401(423)}$
Asp^{11}	Arg$^{397(419)}$
Asp^{12}	Arg$^{397(419)}$

ITAM Recognition—All ITP amino acids corresponding to fingerprint residues defining the ITAM (Glu^2, Tyr^5, and Leu^8) or to residues conserved in the CD79a ITAM region (Leu^4, Glu^6, and Gly^7) (11, 51) interact either through hydrogen bonding or by hydrophobic contacts with kinase residues (Table III) that are also highly conserved among Src kinases (52). That these intermolecular interactions may be important recognition determinants is supported by the binding preferences of Lyn identified by peptide libraries and phage display studies (53, 54). The combined substrate sequences indicate preferences for the position P−3, P−1, P+1, and P+3 (Scheme 1). Some of these interactions are shown in Fig. 6. We note in particular Leu^8 (P+3), which is buried at the interface of the N- and C-lobes (Fig. 6, *A* and *D*) by hydrophobic contact with kinase residues Leu$^{385(407)}$, Gly$^{399(421)}$, Ala$^{400(422)}$, and Phe$^{402(424)}$. Leu^8 methyl resonances are shifted by 0.03 ppm upon binding, and the burial of Leu^8 deep in a hydrophobic region of the cleft is consistent with this chemical shift perturbation. CD79a ITAM residue Leu^4 (P−1) has hydrophobic contacts with Tyr^5 and Phe$^{256(278)}$, a highly conserved kinase residue, while Glu^6 (P+1) hydrogen-bonds with Gln^{255} (Cys^{277}). The lack of conservation among the Src family kinases at this position could provide a basis for Lyn and Lck binding selectivity. We note that there is extensive intermolecular interactions between ITP and the phosphorylated activation segment. Such interaction suggests that phosphorylation of the activation segment

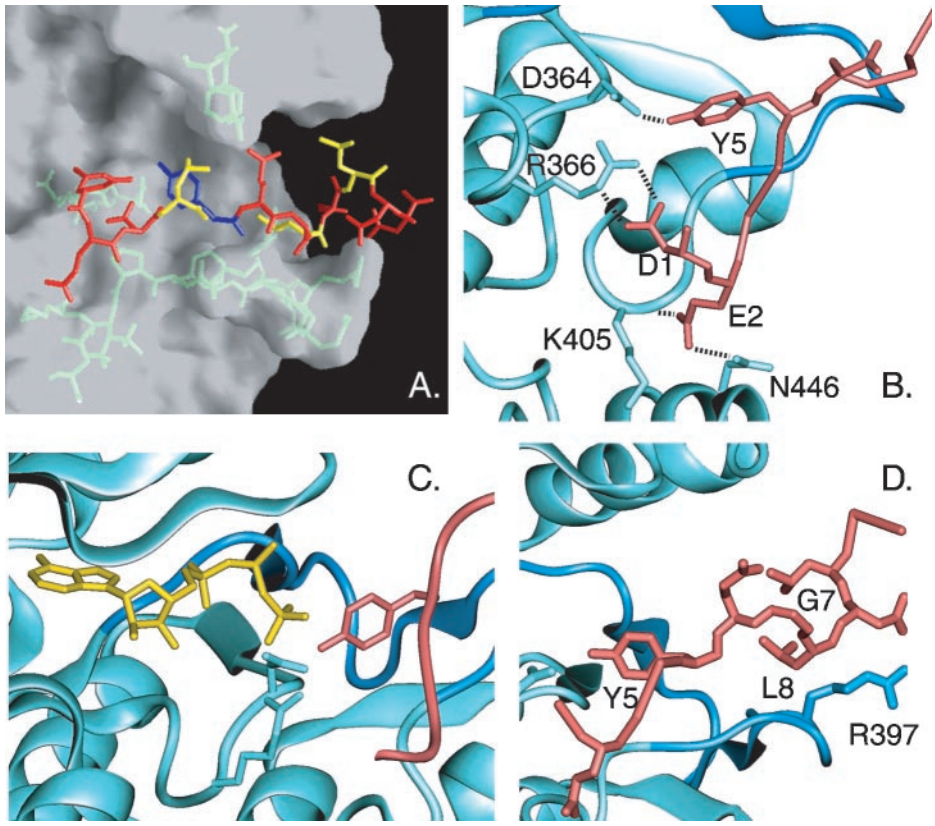

FIG. 6. **Interactions of the ITP acet-(DENLYEGLNLDD)-NH_2 NMR structure modeled in the cleft between the N- and C-lobes of kLck.** Residues three away from the acceptor Tyr, P+3 and P−3, are part of the ITAM fingerprint. *A*, transparent molecular surface of kLck showing the enzyme residues in contact with ITP and the steric complementarity between the substrate and enzyme. The acceptor Tyr is colored *blue*, Leu residues are colored *yellow*, and polar residues are colored *red*. *B*, view of the active site kLck residues $Asp^{364(386)}$ and $Arg^{366(388)}$ with hydrogen bonds to ITP Tyr^5 and Asp^1. ITP Glu^2 (P−3) hydrogen bonds to kLck residues $Lys^{405(427)}$ and $Asn^{446(468)}$. *C*, ATP (not included in the modeling of ITP to kLck) is overlaid on the ITP-kLck model showing the reasonable position for catalysis. *D*, ITP residues Gly^7 (P+2) and Leu^8 (P+3) bind in the cleft. Gly^7 adapts a main chain conformation energetically favorable only for glycine. The activation segment is colored *dark blue*, and ITP is colored *red* in *B–D*.

plays an active role in substrate binding as opposed to only eliminating a steric barrier to binding.

ITAM Substrate Specificity—The model of the ITP complex gives insight into the substrate specificity of Lyn for the CD79a ITAM. The ITAM includes two Tyr residues (Scheme 1). The first Tyr residue of the ITAM is the major site phosphorylated by Lyn upon activation of the signaling pathway in immune cells, while the second Tyr is less extensively phosphorylated (8–10). *In vitro*, Lyn demonstrates a strong preference for phosphorylation of the NH_2-terminal Tyr (Fig. 1). The sequence of the CD79a ITAM near the two Tyr residues is *YXXL* for both, but differs at the P−3 and P+2 positions; these positions for the first and second Tyr are Glu *versus* Cys, and Gly *versus* Asp, respectively. Glu^2 has strong interactions through side chain hydrogen bonds in the modeled complexes (Table III). These interactions cannot be accommodated by the Cys residue at the P−3 position from the second Tyr of ITAM. A second factor distinguishing the first Tyr for phosphorylation is the conformation of Gly^7 at the P+2 position; the main chain conformation of Gly^7 has (ϕ,ψ) values that fall in a region of the Ramachandran plot energetically favorable only for glycine residues in order to accommodate extensive contact of both Tyr^5 and Leu^8 in the cleft. It is worth noting that this β-turn-like feature of Gly^7 for bound ITP occurs in the NMR structures determined as the isolated ITP, and is not generated by docking.

The roles of Glu^2 (P−3) and Gly^7 (P+2) in substrate recognition by Lyn were examined by measuring K_m values for peptide variants of ITP. Peptides were synthesized with the ITP sequence except that Glu^3 was replaced with Ala (ITP-E3A), or Gly^7 was replaced with Thr (ITP-G7T). K_m was measured using the enzymatic assay described under "Experimental Procedures." Binding of ITP-E3A was not detected under the conditions of the assay, which suggests that the hydrogen-bonding interactions of this group are important for binding. In the case of ITP-G7T, K_m is 10 μM, similar to the ITP value of 13 μM. The lack of an effect on K_m suggests that the conformational flexibility of Gly^7 is not critical for binding, at least within the context of the peptide model.

Kinase Activation—By binding in the cleft between the N- and C-lobes of the kinase domain, ITP could serve to stabilize the most catalytically active form of the enzyme. Activation of kinases appears to depend in part on the orientation of the N- and C-lobes of the kinase domain, as concluded by comparison of numerous crystallographic structures for various forms and ligation states of these enzymes (19, 45, 46, 55). If the inactive form of Hck or Src is compared with the active form of Lck, the lobe-lobe orientation of the active form being more open (Fig. 4). A least-squares fit of the N-lobe after superposition of the C-lobe requires a 13° rotation. The internal structure of each lobe remains roughly constant between active and inactive forms of Src family kinases (0.8- and 1.0-Å main chain root mean square difference after superposition of either the N-lobe or C-lobe, respectively). Thus, the relative lobe movement is largely a rigid body motion. One distinction between the lobe structures is displacement of two helices: α-C in the N-lobe (42, 43) and α-G in the C-lobe. It is of interest to note that the modeled ITAM substrate contacts both of these helices (described below). Further, ATP binding does not appear to depend on the lobe-lobe orientation since down-regulated apo-Hck and Src complexed with an ATP analogue have similar lobe-lobe orientation. Although the exact consequence of the lobe orientations on catalysis is not fully understood, the differences observed in the crystallographic structures of various kinase forms strongly suggest that the lobe-lobe displacement is tightly coupled to activation.

The extensive interactions between the cleft-bound ITAM substrate and both lobes of the kinase domain would serve to stabilize the orientation of the two lobes most appropriate for enzymatic catalysis. Specifically, the ITAM substrate contacts the N-lobe at the nucleotide binding loop, the β3-αC loop, and the amino terminus of α-C. In regard to the C-lobe, extensive

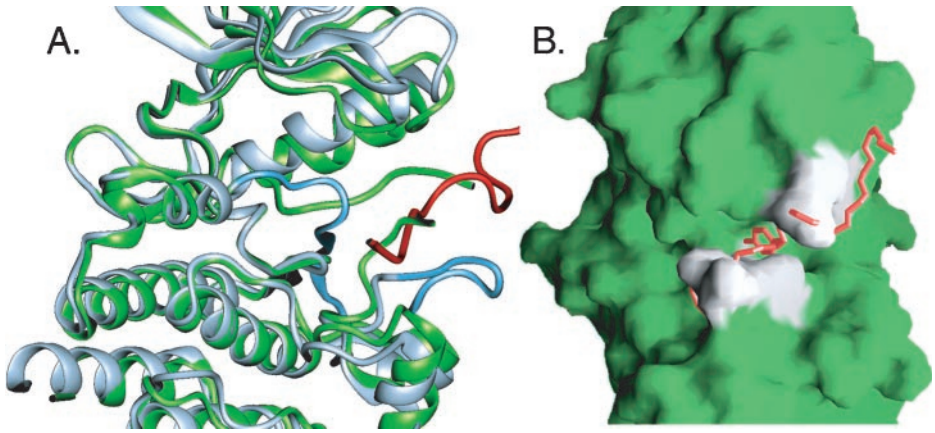

FIG. 7. **Steric conflict between ITP substrate, modeled in the cleft of the active form of the Src family kinase, with the activation segment from the inactive form.** The structures of the two forms of the kinase are overlaid as in Fig. 2. *A*, ribbon drawing of inactive Hck (*green*) and activated kLck (*blue*) with ITP (*red*). The ends of the Hck activation segment overlap the space occupied by ITP. *B*, molecular surface of inactive Hck showing the position of the activation segment (*white*) and ITP (*red bonds*). (View is rotated relative to *A*.)

contact by substrate is made with the activation segment, and the amino terminus of α-G helix. The model suggests that ITAM substrate would not bind the down-regulated kinase because the narrower width of the cleft between the two lobes, and the altered positions of α-C and α-G would not optimally accommodate the substrate. A second factor to block binding of the ITAM substrate to the inactive form of the Src family kinase is the substantial steric conflict that arises between the ITAM substrate and the activation segment of the unphosphorylated state. The conflict, illustrated in Fig. 7*A* by overlay of the C-lobes of inactive Hck and activated kLck, occurs between ITP and the activation segment of Hck, residues 409–411 and 422–425, near the region where the electron density is lost due to disorder in this structure. Rotation of the view in Fig. 7*A* and visualization of the molecular surface in Fig. 7*B* clearly illustrate the penetration by ITP residues of the space occupied by the Hck activation segment (colored *white* in Fig. 7*B*). This steric clash is even more extensive in the recently determined Src and Hck down-regulated structures with a fully defined activation segment.

Conclusions—As the first structure of a Src family kinase substrate bound to an active form of the enzyme, the et-NOE structure of the ITAM peptide from the B cell antigen receptor shows that Src kinase substrates bind in an extended, irregular helical conformation. Given the importance of the Src kinases in signaling and their implication in human disease, it is our hope that these results provide a structural basis for the design of potential inhibitors.

Modeling the ITAM peptide on the surface of kLck strongly suggests the ITAM substrate binds in the cleft between the N- and C-lobes of the catalytic domain. In the cleft-binding mode, all conserved CD79a ITAM residues near the first Tyr residue (Table III) are engaged in intermolecular interactions, and the ITAM substrate contacts protein regions that are highly conserved among protein kinases. ITAM binding in the cleft implies that substrate recognition is associated with stabilizing the active form of the kinase, in contrast to the ATP cofactor, which can bind the inactive form of Src family kinase. The ITAM contact region spans both lobes by interactions with the phosphorylated activation segment, the nucleotide binding loop, and the α-helices C and G, all kinase regions implicated in activation or catalysis. Thus, the model of the kinase-substrate complex presented here strongly suggests that substrate recognizes the activated form of the Src family kinase with respect not only to the conformation of the activation segment, but also to the orientation of the N- and C-lobes in the catalytic domain. Recognition of a certain interlobe orientation optimal for enzymatic catalysis has implications on controlling enzymatic activity through domain-domain interactions of the catalytic domain with the SH2 or SH3 domains (45, 56). Another noteworthy outcome of the modeled complex is the predicted basis for the observed preference of Lyn to phosphorylate the amino-terminal Tyr residue in the CD79a ITAM over the carboxyl-terminal Tyr. One important factor for recognition appears to be hydrogen-bonding interactions of Glu at the position P−3 from the acceptor site. Gly at the P+2 position binds with a main chain conformation that is energetically favorable only for glycine, but this feature was not essential for recognition within the context of a peptide substrate.

Acknowledgments—We thank Dr. A. LiWang, Chris Issacson, Uyen Ngo, and LaTisha White for their assistance.

REFERENCES

1. Reth, M. (1989) *Nature* **338,** 383–384
2. Cambier, J. C. (1995) *J. Immunol.* **155,** 3281–3285
3. Isakov, N. (1997) *J. Leukocyte Biol.* **61,** 6–16
4. Yamanashi, Y., Fukushige, S.-I., Semba, K., Sukegawa, J., Miyajima, N., Matsubara, K.-I., Yamamoto, T., and Toyoshima, K. (1987) *Mol. Cell. Biol.* **7,** 237–243
5. Yi, T., Bolen, J. B., and Ihle, J. N. (1991) *Mol. Cell. Biol.* **11,** 1398–2391
6. Yamanashi, Y., Kakiuchi, T., Mizuguchi, J., Yamamoto, T., and Toyoshima, K. (1991) *Science* **251,** 192–194
7. Burg, D. L., Furlong, M. T., Harrison, M. L., and Geahlen, R. L. (1994) *J. Biol. Chem.* **269,** 28136–28142
8. Saouaf, S. J., Mahajan, S., Rowley, R. B., Kut, S. A., Fargnoli, J., Burkhardt, A. L., Tsukada, S., and Witte, O. (1994) *Proc. Natl. Acad. Sci. U. S. A.* **91,** 9524–9528
9. Nagai, K., Takata, M., Yamamura, H., and Kurosaki, T. (1995) *J. Biol. Chem.* **270,** 6824–6829
10. Johnson, S. A., Pleiman, C. M., Pao, L., Schneringer, J., Hippen, K., and Cambier, J. C. (1995) *J. Immunol.* **155,** 4596–4603
11. Flaskwinkel, H., and Reth, M. (1994) *EMBO J.* **13,** 83–89
12. Pao, L. L., Famiglietti, S. J., and Cambier, J. C. (1998) *J. Immunol.***160,** 3305–3314
13. Rowley, R. B., Burkhardt, A. L., Chao, H.-G., Matsueda, G. R., and Bolen, J. B. (1995) *J. Biol. Chem.* **270,** 11590–11594
14. Reth, M., and Wienands, J. (1997) *Annu. Rev. Immunol.* **15,** 453–479
15. Levitzki, A., and Gazit, A. (1995) *Science* **267,** 1782–1788
16. Bolen, J. B., and Brugge, J. S. (1997) *Annu. Rev. Immunol.* **15,** 371–404
17. Yamaguchi, H., and Hendrickson, W. A. (1996) *Nature* **384,** 484–489
18. Knighton, D. R., Zheng, J., Ten Eyck, L. F., Xuong, N.-H., Taylor, S. S., and Sowadski, J. M. (1991) *Science* **253,** 414–423
19. Hubbard, S. R. (1997) *EMBO J.* **16,** 5572–5581
20. Guan, K., and Dixon, J. E. (1991) *Anal. Biochem.* **192,** 262–267
21. West, M. H. P., Wu, R. S., and Bonner, W. M. (1984) *Electrophoresis* **5,** 133–138
22. Barker, S., Kassel, D. B., Weigl, D., Huang, X., Luther, M., and Knight, W. B. (1995) *Biochemistry* **34,** 14843–14851
23. Dhalluin, C., Wieruszeski, J.-M., and Lippens, G. (1996) *J. Magn. Res. Ser. B* **111,** 168–179
24. Bax, A., and Davis, D. G. (1985) *J. Magn. Res.* **63,** 207–213
25. Piotto, M., Saudek, V., and Sklenar, V. (1992) *J. Biomol. NMR* **2,** 661–665
26. Delaglio, F., Grzesiek, S., Vuister, G., Zhu, G., Pfeifer, J., and Bax, A. (1995) *J. Biomol. NMR* **6,** 277–293
27. Kraulis, P. J. (1989) *J. Magn. Res.* **84,** 627–633
28. Brunger, A. T. (1992) *X-PLOR*, version 3.1,Yale University Press, New Haven, CT
29. MacKerell, A. D. J., Bashford, D., Bellott, M., Dunbrack, R. L., Evanseck, J. D., Field, M. J., Fischer, S., Gao, J., Guo, H., Ha, S., JosephMcCarthy, D., Kuchnir, L., Kuczera, K., Lau, F. T. K., Mattos, C., Michnick, S., Ngo, T., Nguyen, D. T., Prodhom, B., Reiher, W. E., Roux, B., Schlenkrich, M., Smith, J. C., Stote, R., Straub, J., and Karplus, M. (1998) *J. Phys. Chem. B* **102,** 3586–3616
30. Laskowski, R. A., MacArthur, M. W., Moss, D. S., and Thornton, J. M. (1995) *J. App. Crystallogr.* **26,** 283–291

31. Brooks, B. R., Bruccoleri, R. E., Olafson, B. D., States, D. J., Swaminathan, S., and Karplus, M. (1983) *J. Comput. Chem.* **4,** 187–217
32. Clore, G. M., and Gronenborn, A. M. (1983) *J. Magn. Reson.* **53,** 423–442
33. Onoda, T., Iinuma, H., Sasaki, Y., Hamada, M., Isshiki, K., Naganawa, H., Takeuchi, T., Tatsuta, K., and Umezawa, K. (1989) *J. Nat. Prod.* **52,** 1252–1257
34. Hsu, C.-Y. J., Persons, P. E., Spada, A. P., Bednar, R. A., Levitzki, A., and Zilberstein, A. (1991) *J. Biol. Chem.* **266,** 21105–21112
35. Eisenmesser, E., Zabell, A., and Post, C. B. (2000) *J. Biomol. NMR*, in press
36. Schneider, M. L., and Post, C. B. (1995) *Biochemistry* **34,** 16574–16584
37. Sternberg, M. J. E., Bates, P. A., Kelley, L. A., and MacCallum, R. M. (1999) *Curr. Opin. Struct. Biol.* **9,** 368–373
38. Venclovas, C., Ginalski, K., and Fidelis, K. (1999) *Proteins Struct. Funct. Genet.* Suppl. 3, 73–80
39. Koehl, P., and Levitt, M. (1999) *Nat. Struct. Biol.* **6,** 108–111
40. Sali, A. (1998) *Nat. Struct. Biol.* **5,** 1029–1032
41. Wei, L., Hubbard, S. R., Smith, R. F., and Ellis, L. (1994) *Curr. Opin. Struct. Biol.* **4,** 450–455
42. Sicheri, F., Moarefi, I., and Kuriyan, J. (1997) *Nature* **385,** 602–609
43. Xu, W., Harrison, S. C., and Eck, M. J. (1997) *Nature* **385,** 595–602
44. Williams, J.-C., Weijland, A., Gonfloni, S., Thompson, A., Courtneidge, S.-A., Superti-Furga, G., and Wierenga, R. K. (1997) *J. Mol. Biol.* **274,** 757–775
45. Schindler, T., Sicheri, F., Pico, A., Gazit, A., Levitzki, A., and Kuriyan, J. (1999) *Mol. Cell* **3,** 639–648
46. Xu, W., Doshi, A., Lei, M., Eck, M. J., and Harrison, S. C. (1999) *Mol. Cell* **3,** 629–638
47. Nicholls, A., Sharp, K. A., and Honig, B. (1991) *Proteins* **11,** 281–296
48. Zheng, J., Knighton, D. R., Ten Eyck, L. F., Karlsson, R., Xuong, N.-H., Taylor, S. S., and Sowadski, J. M. (1993) *Biochemistry* **32,** 2154–2161
49. Lowe, E. D., Noble, M. E. M., Skamnaki, V. T., Oikonomakos, N. G., Owen, D. J., and Johnson, L. N. (1997) *EMBO J.* **16,** 6646–6658
50. Huse, M., Chen, Y.-G., Massague, J., and Kuriyan, J. (1999) *Cell* **96,** 425–436
51. Keegan, A. D., and Paul, W. E. (1992) *Immunol. Today* **13,** 63–68
52. Hanks, S. K., Quinn, A. M., and Hunter, T. (1988) *Science* **241,** 42–52
53. Ruzzene, M., Songyang, Z., Marin, O., Donella-Deanna, A., Brunati, A. M., Guerra, B., Agostinis, P., Cantley, L. C., and Pinna, L. A. (1997) *Eur. J. Biochem.* **246,** 433–439
54. Schmitz, R., Baumann, G., and Gram, H. (1996) *J. Mol. Biol.* **260,** 664–667
55. Williams, J. C., Wierenga, R. K., and Saraste, M. (1998) *Trends Biochem. Sci.* **23,** 179–184
56. Salemme, F., Spurlino, J., and Bone, R. (1997) *Curr. Opin. Struct. Biol.* **5,** 319–324